PCCP

Accepted Manuscript

ROYAL SOCIETY OF CHEMISTRY

www.rsc.org/pccp

PCCP

RSCPublishing

Perspective

Physicochemical design and analysis of self-propelled objects that are characteristically sensitive to environments

Cite this: DOI: 10.1039/x0xx00000x

Received 00th January 2012,
Accepted 00th January 2012

DOI: 10.1039/x0xx00000x

www.rsc.org/

Satoshi Nakata,[*a] Masaharu Nagayama,[bc] Hiroyuki Kitahata,[d] Nobuhiko J. Suematsu,[ef] Takeshi Hasegawa[g]

The development of self-propelled motors that mimic biological motors is an important challenge for the transport of either themselves or some material in a small space, since biological systems exhibit high autonomy and various types of responses, such as taxis and swarming. In this Perspective, we review non-living systems that behave like living matter. We especially focus on nonlinearity to enhance autonomy and the response of the system, since characteristic nonlinear phenomena, such as oscillation, synchronization, pattern formation, bifurcation, and hysteresis, are coupled to self-motion of which driving force is the difference in the interfacial tension. Mathematical modelling based on reaction-diffusion equations and equations of motion as well as physicochemical analysis from the point of view of the molecular structure are also important for the design of non-living motors that mimic living motors.

1. Introduction

Many self-propelled systems, e.g., noble metals or modified solid materials based on catalytic reactions in solutions,[1-3] liquid droplets[4-9] or solid grains[2,3,10,11] at interfaces, have been investigated with respect to their ability to transport either themselves or some material within a micro- to centimeter-scale space without the application of an external force. However, the features of this motion seem to be restricted. For example, the direction of motion for a liquid droplet on a solid surface is determined by the difference in the contact angle which is generated by the chemical gradient.[5-7] In other examples, the direction of motion for various substances is controlled by external electromagnetic fields.[12,13]

On the other hand, prokaryotes, such as a bacterium, can spontaneously and variously change the direction, speed, and behaviour of motion within a small space while responding to the environment or physicochemical stimuli, i.e., taxis.[14] Thus, the enhancement of autonomy and diversity of the response are important concerns in creating non-living systems that mimic living systems. The coupling of nonlinear phenomena with such systems is an idea for enhancing autonomy and the diversity of the response since living systems exhibit utilize nonlinear phenomena, such as oscillation, bifurcation, synchronization, spatio-temporal pattern formation, and so on.[8,15-17]

In this Perspective, we review non-living systems for which the driving force is a difference in interfacial tension. For example, a camphor grain or a camphor boat spontaneously moves on water.[10,11,18] We especially focus on features of motion that characteristically depend on the environment and physicochemical stimuli from the viewpoint of nonlinearity. Figure 1 shows a schematic illustration of the scope of this Perspective.

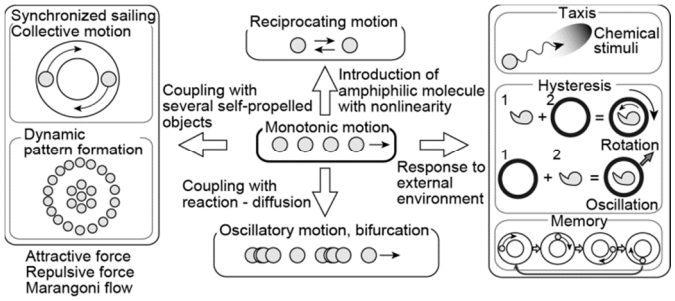

Fig.1 Schematic illustration of the characteristic features of self-propelled objects that can be designed by coupling with nonlinear phenomena, through molecular structures, reaction-diffusion dynamics, external environment, and mutual interaction.

2. Self-propelled systems at interfaces

In this chapter, we review characteristic motion of camphor systems depending on the shape of water channel, plastic boat, and camphor grain. Synchronization and collective motion can be realized by coupling of several camphor disks or boats on an annular water channel. In addition, we mention the effect of Marangoni flow to

self-propelled systems since Marangoni flow is driven by the difference in the interfacial tension. As for the related studies, we mention characteristic motion coupled with spatio-temporal pattern and chemotaxis of a droplet based on a nonlinear reaction and nonequilibirum condition. Then, we mention the effect of molecular structure on self-motion.

2.1 Camphor systems sensitive to the environment

A camphor system is a simple and readily available self-propelled system since it is easy to prepare a camphor grain or a camphor boat in a desired shape as the internal condition and the shape of the water chamber as the external condition. The self-motion of a camphor grain was first reported more than a century ago and the basic principle of the motion was elucidated, i.e., the driving force was a difference in the surface tension.[10,11] Since the shape of a natural camphor grain is complicated and changes with time due to sublimation and dissolution, it has been difficult to characterize the complicated features of motion. Thus, by controlling the shape of a camphor grain or a camphor boat, we can control the direction of motion. However, such shape-control only induces unidirectional translation or rotation.[18] In this section, we show that camphor exhibits characteristic motion depending on the configuration of the system itself.

Ideally, if a camphor disk as a symmetric self-propelled object is placed on water, it should not move, since the surface tension around the disk is balanced due to the isotropic distribution of camphor molecules around it. However, since this isotropic distribution is actually broken by slight anisotropy of the initial floating state, the camphor disk can start to move.[19] This motion of camphor maintains the anisotropic distribution of camphor molecules, and therefore the camphor disk can maintain unidirectional motion. A similar phenomenon of symmetry-breaking depending on the initial motion was reported for ethanol-soaked PNIPAm gels with characteristic shapes.[20]

When a camphor disk is placed in a linear water channel, reciprocating motion without collision with the channel is generated.[21,22] Reciprocating motion is caused by inversion of the spatial gradient of the camphor concentration around the camphor disk due to the presence of the edges of the water channel, as shown in Fig. 2. Thus, spontaneous symmetry-breaking induces reciprocating motion with sensing of the boundary.

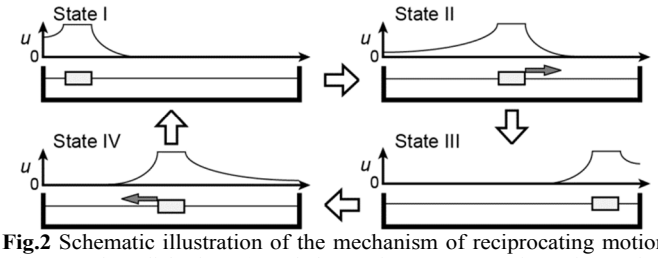

Fig.2 Schematic illustration of the mechanism of reciprocating motion of a camphor disk (lower) and the surface concentration of camphor molecules, *u* (upper). States I, II, III, and IV are repeated.[21,22]

A camphor boat moves to the region with the higher surface tension, i.e., the direction opposite to the side of the boat attached to the camphor grain. The camphor boat can maintain unidirectional motion for at least 30 min. This means that the difference in the surface tension around the boat is maintained because of the sublimation and dissolution of the camphor molecules developed to the water surface. When a plastic film, which is attached to a camphor disk on its bottom surface, is placed on water, mode-bifurcation between continuous motion and oscillatory motion is generated as a function of the location of the camphor disk.[23,24] Oscillatory motion is due to repetition between the diffusion of camphor molecules under the film in the resting state and the development of camphor molecules on water in the moving state. Thus, the period of oscillatory motion decreases, and oscillatory motion (Fig.3-2) bifurcates to give continuous motion (Fig.3-1) with an increase in the distance between the center of the boat and the central position of the camphor disk.

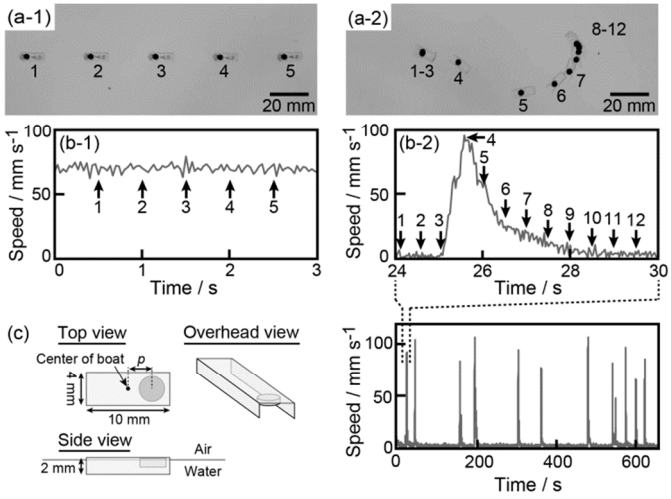

Fig.3 Mode-bifurcation of a camphor boat depending on the location of a camphor boat (p = (1) 3.0 and (2) 0.0 mm).[23,24] (a) Superimposed image of snapshots of the camphor disk (time interval: 0.5 s), (b) time-course of the speed of camphor motion, and (c) schematic illustration of the camphor boat and definition of p.

In related work on oscillatory motion that is based on the diffusion rate of the substance that is the source of the driving force, Sharma et al. reported periodic pulsating motion of an ethanol-infused hydrogel in a plastic tube on water.[25] Such periodic motion is based on the spontaneous oscillation of surface tension, which has been investigated by Kovalchuk et al.[26]

When a self-propelled object that exhibits oscillatory motion (alternating between motion and rest) in an annular water channel, motion with memory is generated.[27] Thus, the resting positions and features of motion in subsequent cycles are almost the same as those observed previously. The occurrence of this memory phenomenon depends on the relationship between the resting duration and the period for one lap of the annular channel. In the related work on motion with memory, Santos et al. reported that an *n*-alkane droplet that contains silane molecules moves on a glass surface while escaping its trajectory.[28]

2.2 Effect of the shape a camphor grain on its self-propelled motion

In this section, we describe the effect of the shape of a camphor grain on motion and discuss the relationship between the symmetry of the system and motion. We can classify self-propelled objects into two types from the viewpoint of symmetry: asymmetric objects, for which the direction of motion is determined by their intrinsic asymmetry, and symmetric objects, which move through spontaneous symmetry-breaking. A camphor boat in which a camphor disk is attached to the edge of a plastic boat is an example of the former type, while a camphor disk is an example of the latter type.

We can control the motion of a camphor grain by designing its shape. It has been reported that a camphor grain with a boomerang-like shape exhibits translational motion, while a comma-shaped camphor grain exhibits rotational motion.[18] These camphor grains are classified as asymmetric objects.

An interesting topic in the field of active matter is the coupling between motion and deformation. In this sense, most fundamental deformation is elliptic deformation. Ohta and Ohkuma proposed a model in which motion and elliptic deformation are coupled with each other.[29] Inspired by their work, we can ask a simple but nontrivial question; In which direction does an elliptic camphor grain move? To address this question, we performed a theoretical analysis, and found that such a grain moves in the direction of its short-axis. The experimental and numerical results are consistent with the analytical results.[30,31] A camphor grain has an advantage in that we can give it an arbitrary shape. We hope to design the other shapes so that we can discuss important fundamental problems regarding active matters.[20]

2.3 Synchronized swimming and collective motion

When two or more oscillators are coupled together, the phase difference between them can be constant. This typical nonlinear phenomenon is called "synchronization".[17,32] Synchronization can be observed in living organisms, such as in the beating heart, circadian rhythm, the organized rhythm in the flashing of swarms of fireflies, and so on.[16] Self-propelled systems also show synchronization and often exhibit several types of ordered patterns and functional behaviours. Such behaviours are referred to as "collective motion". Living things often show collective motion, e.g., flocks of birds, schools of fish, and colonies of bacteria.[33] An understanding of self-propelled systems should be useful for elucidating the mechanism of collective motion in living systems. In this section, we describe the synchronized sailing of two or more camphor disks or boats when they are placed on the same water channel.

A camphor boat consists of a thin plastic plate and a solid camphor disk. If the disk is attached to one end of the plate, the boat has a direction to move. When two equivalent camphor boats are placed so that they move in the same direction on an annular water channel, two synchronized motions are observed depending on the water temperature;[34] i.e., phase-locking and phase-oscillatory synchronization are generated at lower and higher temperatures, respectively. These boats interact through the surface concentration field of camphor. Thus, the distribution of camphor molecules that develop from the solid camphor plays an important role in the features of synchronization.

The surface concentration of camphor decreases exponentially with distance from the edge of the camphor disk.[35] Thus, the camphor boat approaches the other boat, and the driving force decreases due to the lower surface tension at the front of the first boat. This effect makes the boats move away from each other. When the decay length of the surface concentration is large, the two boats always affect each other. Since an equivalent concentration gradient between the camphor boats induces an equivalent driving force, the phase difference reaches π rad as a stable state (phase-locking synchronization). On the other hand, sublimation and dissolution of camphor molecules on water is enhanced at a higher temperature, which disrupts the stable state and induces phase-oscillatory synchronization. In other synchronized systems, two equivalent camphor boats exhibit characteristic synchronized motion depending on the shape of a polygonal or figure-eight water chamber.[36,37]

Bifurcation of the mode of collective motion is also observed in a multiple-body system. When several camphor boats are placed on an annular water channel, the speed of the boats remains constant over time and the boats are distributed homogeneously throughout the entire channel. This mode corresponds to phase-locking as is described above, where the phase difference becomes $2\pi/n$ (n: number of camphor boats). The phase-locking mode becomes unstable over a threshold number of boats, where the boats show an inhomogeneous distribution. In this mode, the speed of each boat oscillates and phase-oscillatory synchronization appears.[38] This type of the bifurcation has the same appearance as the traffic flow of vehicles.[40] Mathematical analyses also revealed that the collective motion of camphor boats has the same type of mathematical structure as traffic flow.[38,40] In addition to the phase-locking and phase-oscillation modes, clustering behaviour is also observed in a collection of camphor boats in an annular channel.[38] Here, several boats move together as an aggregate. This behaviour can be understood in terms of the surface concentration profile of camphor. Heisler et al. clearly showed how to realise clustering behaviour in the collective motion of camphor boats.[41] Their numerical approach revealed that the aggregation of camphor boats often becomes stable and thus clustering behaviour is observed.

With the use of solid camphor disks without a plastic boat, a collection of disks shows other types of bifurcation behaviour depending on the population.[42,43] Heisler et al. used a mathematical model and showed that camphor disks on an annular water channel exhibit several types of behaviour. They reported three types of collective motion, which appeared depending on the population of the disks and the friction coefficient.[42] With a high friction coefficient, the disks are stationary. A decrease in the friction coefficient induces motion of the disk. At a mid-range friction, the disks

repeatedly show motion and collision, where the spatial symmetry of the motion is maintained throughout the entire system. However, symmetry is spontaneously broken at a lower value for the friction coefficient. Under this condition, all of the disks move either clockwise or counter-clockwise.

Such symmetry-breaking behaviour has been demonstrated by Ikura et al. They prepared circular camphor paper disks and placed them on an annular water channel.[43] With a low disk population, continuous motion is observed, where all of the disks move in the same direction. Thus, symmetry is broken (Fig. 4a). With an increase in the population, the continuous motion changes to alternation between rest and motion. Two types of the alternating behaviour are observed: billiard-type and catch and release-type. In the former, almost all of the camphor disks are stationary with a constant distance between them and only a few disks move. A moving disk collides with its neighbour and then becomes stationary while the neighbouring disk starts to move (Fig. 4b). During this motion, the other disks are stationary. Therefore, collision point propagates in the same direction as the direction of motion. This type of behaviour is observed in a mid-sized population. With a further increase in the population, the behaviour changes to the other type of alternation, where almost all of the camphor disks form a stationary cluster and only one or two disks shift from the front to the tail of the closely packed cluster (Fig. 4c).

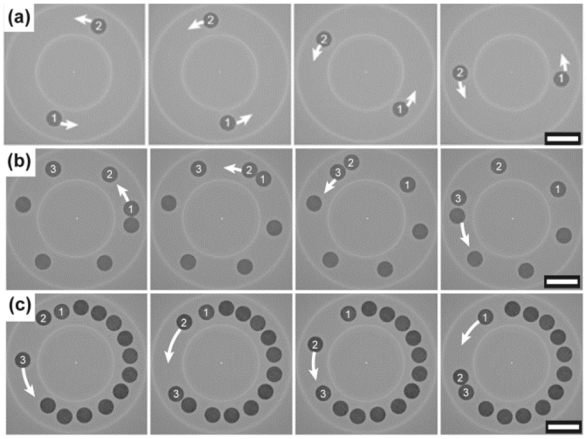

Fig. 4 Experimental observation of collective behaviours of camphor disks in an annular water channel. (a) Unidirectional motion of two camphor disks. (b) Billiard-type alternation of camphor disks with a mid-range population. (c) Catch and release-type alternation in the high population range. Time intervals in the snapshots are (a, c) 0.30 and (b) 0.36 s. Reprinted with permission from [43]. Copyright 2013 American Physical Society. White scale bars were 20 mm.

For a circular water chamber such as a Petri dish, the direction of motion of camphor disks is not restricted to simply the left or right. Therefore, other types of collective motion, including the spatial arrangement of disks, are observed. Soh et al. reported that camphor-soaked gel particles, which are round or rectangular, show arrangement of the direction of motion similar to swarming behaviour or formed a stationary ordered lattice pattern with a constant distance between the particles (Fig. 5a).[44,45] The former behaviour is observed in the case of a low population of camphor; in contrast, the latter is seen with a high population. These characteristic collective motions arise due to the interaction between camphor gel particles. Soh et al. also numerically investigated the interaction between the camphor particles on a wide water surface based on the convective flow which is induced by the Marangoni effect. (The effect of convective flow is described in Section 2.4) Their calculations revealed that camphor disks can show both attractive and repulsive interactions, and this depends on the water depth (Fig. 5b). Based on such interactions, alignment of the direction of motion and a spatial ordered pattern formation are realized.[44,45] In addition to such spatial structures, we found rhythmic collective motion of camphor gel disks, which was composed of short-time rapid motion and long-time stationary state.[46]

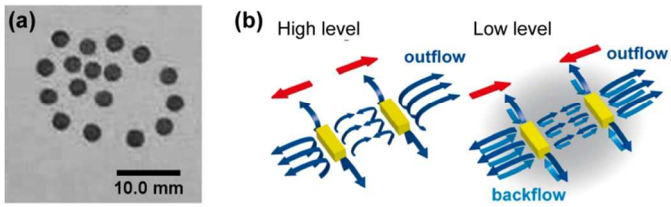

Fig. 5 (a) Experimental observation of arrangement pattern of camphor disks. (b) Schematic image of the interaction working between the camphor disks based on convective flow. Reprinted with permission from [45]. Copyright 2011 American Chemical Society.

In other camphor systems, Markus reported on four types of spatial distribution of dynamic ensembles of camphor particles on water: no clustering, clustering, net-like structure, and no motion.[47]

Taylor's group investigated the self-motion of aspirin crystals which exhibited characteristic interactive motion depending on the pH of the aqueous phase.[48] They discussed on the characteristic phenomena in relation to the capillary interaction and Marangoni effects.

2.4 Effect of convection

In this section, we describe the relationship between self-propelled motion and Marangoni flow, which is induced by a difference in the interfacial tension.[49]

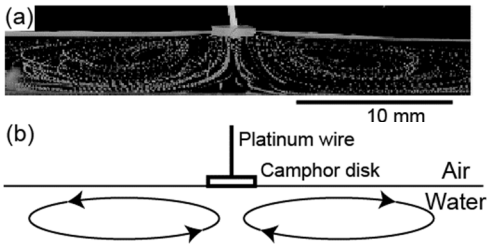

Fig. 6 Experimental observation of Marangoni convection, where a camphor disk is attached to the water surface in a quasi-two-dimensional chamber. To visualize Marangoni convection, small particles ((DIAION, HP20S, Mitsubishi Chemical Co., Tokyo, Japan; particle size 100-200 μm) are distributed in the water phase.[50,51] (a) Superposed images over 1 s. (b) Schematic illustration to show the configuration, and the direction of convective flow. Reprinted with permission from [51]. Copyright 2012 American Chemical Society.

When a camphor disk is placed on water, the camphor molecules spread over the surface and reduce the surface tension. Due to the lower surface tension around the camphor disk, Marangoni flow is induced outward from the camphor disk near the water surface. Actually, Marangoni flow was observed experimentally and could affect the spontaneous motion of a camphor disk,[50-53] as shown schematically in Fig. 6. Convective flow was also reproduced based on the Navier-Stokes equation for the flow field and the reaction-diffusion equation for the surface concentration of camphor:[49]

$$\frac{\partial u}{\partial t}+(\mathbf{v}\cdot\nabla)u = D\frac{\partial^2 u}{\partial x^2}-ku+f_0\delta(x), \quad (1)$$

$$\rho\left(\frac{\partial \mathbf{v}}{\partial t}+\mathbf{v}\cdot\nabla\mathbf{v}\right)=\eta\nabla^2\mathbf{v}-\nabla p, \quad (2)$$

$$\nabla\cdot\mathbf{v}=0, \quad (3)$$

where u is the surface concentration of camphor, $\mathbf{v}$ is the fluid velocity, and D, k, f_0, ρ, and η are the diffusion constant, rate constant of the sum of sublimation and dissolution of the developed camphor, supply rate of camphor, fluid density, and fluid viscosity, respectively. Here, we assume that the surface tension, γ, is a decreasing function of the surface concentration u, as

$$\gamma(u)=\frac{a^q(\gamma_0-\gamma_1)}{a^q+u^q}+\gamma_1, \quad (4)$$

where γ_0 and γ_1 are the surface tension of pure water, and the minimum surface tension over the saturated concentration of camphor, respectively. a and q are positive constants. The boundary condition at the bottom of the chamber is a fixed boundary condition, and that at the air-water interface is determined so that the stress balance is satisfied. The profiles of u and flow at the stationary state are shown in Fig. 7.

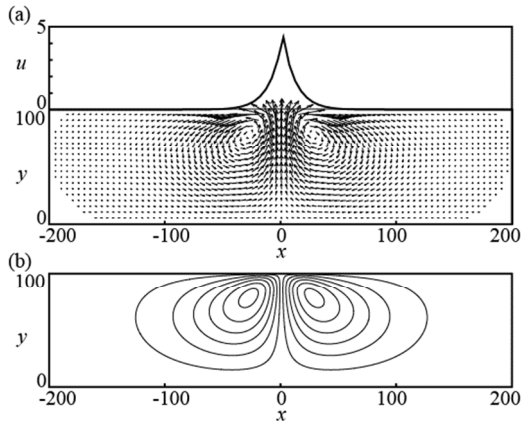

Fig. 7 Numerical results of the stationary state of Marangoni convection.[51-55] The parameters used in the calculation are $D = 1$, $k = 0.01$, $\eta = 100$, $f_0 = 0.1$, $\gamma_0 = 1$, $\gamma_1 = 0$, $a = 1$, and $q = 2$. The calculation area is 400 × 100. (a) Profile of the surface concentration of camphor (upper) and the flow profile (lower). (b) Streamline.

We reported that the convective flow and the contact line around a camphor disk can oscillate when the camphor disk is fixed.[55] This oscillation can be understood in terms of the nonlinear oscillation, and synchronous behaviour can also be seen when two camphor disks are fixed close to each other on water.[56]

We can observe the hysteresis in a camphor system coupled with convective flow.[57] When a camphor grain, which exhibits rotational motion, is placed in a plastic ring, oscillation between rest and motion is generated. On the other hand, the plastic ring rotates in the direction opposite that of the camphor grain when the plastic ring is placed around the rotating camphor grain. These hysteresis behaviours arise due to competition between the generation of rotating convective flow and the development of camphor molecules at the surface.

With addition of a surfactant, e.g., sodium dodecyl sulphate (SDS), to the water phase, the difference in surface tension due to the development of the camphor molecules decreases. Therefore, the magnitude of Marangoni flow is expected to become smaller. However, the magnitude of Marangoni flow is not monotonically dependent on the concentration of the surfactant. With an increase in the concentration of SDS, the magnitude of the flow decreases, but over a threshold concentration, it increases larger again.[51,52]

2.5 Related systems which that exhibit characteristic spatio-temporal motion of a droplet in an aqueous phase

As a related system, a droplet motion coupled with a nonlinear chemical reaction inside it has been reported.[56,57] The Belousov-Zhabotinsky (BZ) reaction is one of the most famous nonlinear chemical reactions, and exhibits spontaneous oscillation in a stirred medium and chemical wave propagation in an unstirred medium. With the use of a ferrous catalyst, the colour of the BZ reaction medium alternates between red and blue, which correspond to reduced and oxidized states, respectively. Due to the difference in surface tension between these two states, a surface tension gradient is induced at the droplet surface, when a chemical wave propagates inside the droplet. This surface tension gradient induces an exchange of momentum through Marangoni convection both inside and outside of the droplet, and the center of mass of the droplet moves coupled with spontaneous pattern formation inside the droplet.[58] In another chemo-mechanical coupling system, Gorecki et al. found that a BZ reactive droplet in an organic phase that included a lipid exhibited periodic changes in the shape of the droplet with a large amplitude. Here, a large amplitude of the shape of the droplet was observed with the use of bathoferroin hexasulfonate as a catalyst since it can induce a large change in interfacial tension.[59] Recently, coupling between cell motion and pattern formation in an area with high protein expression was reported in amoeboid cells, and the BZ droplet system can mimic such cell motion.[60]

In other related systems, oil/water interfaces that exhibit electrochemical oscillation and chemical sensing have been reported.[61-63] A nitrobenzene droplet that contained KI-I_2 exhibits ameba-like motion on the bottom of a Petri dish filled with a cationic surfactant solution.[64-66] Sumino et al. reported the characteristic motion of a nitrobenzene droplet depending

on the shape of the bottom of an aqueous channel.[67] Nanzai et al. found that an *o*-toluidine droplet repeats self-motion between running and squashing as oscillatory motion.[68] These results for droplets suggest that self-propelled motion characteristically responds to the physicochemical environment.

2.6 Chemotaxis

Chemotaxis is a typical motion observed in living things to maintain their lives. In this section, we describe non-living systems that mimic chemotaxis in living systems; e.g., self-propelled objects are characteristically accelerated or decelerated with the addition of chemical stimuli. The motion of a camphor boat changed from constant motion to no motion via oscillatory motion with a decrease in the distance of ester stimulation.[69] A camphoric acid boat is sensitive to the pH of the aqueous phase, i.e., continuous motion changes to oscillatory motion with an increase in pH (details are described in Section 3-1).

In other systems, a mercury droplet can attack an oxidant crystal in a H_2SO_4 or HNO_3 aqueous solution.[70,71] The driving force of motion is the difference in interfacial tension which is locally decreased by oxidation with the dissolved oxidant. The mercury droplet can attack once in the H_2SO_4 solution but many times in HNO_3 due to the production of insoluble Hg_2SO_4 and soluble $HgNO_3$ layers on the mercury surface.

Several kinds of droplets, for which the driving force is the difference in interfacial tension, are sensitive to the concentration gradient of chemical stimuli such as chemotaxis. Ban et al. reported that the motion of a nitrobenzene droplet selectively responds to a rare-earth metal ion, Dy^{3+}.[72] Čejková et al. reported that a decanol droplet moves to a higher concentration of salt.[73] Lagzi et al. reported that an oil droplet composed of dichloromethane and 2-hexyldecanoic acid follows to a pH gradient in the aqueous phase.[74] In fact, these chemotactic droplets can solve a maze.

3. Coupling with chemical reactions and molecular interactions

Cyclic phenomena are important for living organisms. For example, the tricarboxylic acid (TCA) cycle is an important biological chemical reaction for producing energy. In this chapter, we describe how a reaction-diffusion system affects the features of self-propelled motion for which the driving force is a difference in the surface tension.

3.1 Mode-bifurcation depending on the chemical reactions

As an example, we describe coupling with the acid-base reaction.[75-77] When a solid of camphoric acid (R-$(COOH)_2$), as an acid, is placed on a Na_2HPO_4 aqueous solution, as an base, the acid-base reaction (R-$(COOH)_2$ + $2HPO_4^{2-}$ →R-$(COO^-)_2$ + $2H_2PO_4^-$) occurs, where R = C_8H_{14}. The main point of this system is that the source of the driving force is not R-$(COO^-)_2$, but rather R-$(COOH)_2$, since R-$(COOH)_2$ can decrease the surface tension but R-$(COO^-)_2$ cannot. Therefore, the solid camphoric acid nor its boat moves during the reaction. However, the reaction runs to completion due to the consumption of HPO_4^{2-}, and can then be accelerated due to the development of R-$(COOH)_2$ from the solid. As the accelerated camphoric acid solid or its boat moves to another aqueous surface, it rests again because the reaction restarts. Thus, oscillatory motion between rest and motion can be repeated (see Fig. 8). Self-motion changes from continuous motion to no motion *via* oscillatory motion, and the period of oscillatory motion, which corresponds to the resting time, increases with an increase in the concentration of HPO_4^{2-}.

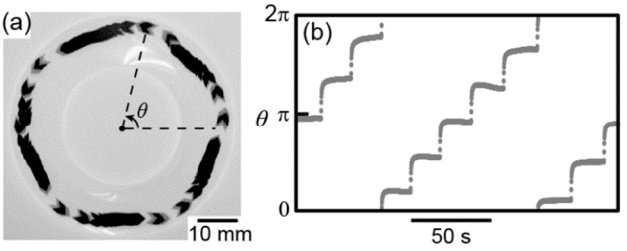

Fig. 8 Self-motion of a camphoric acid boat (acid) on a 0.04 mol L^{-1} Na_2HPO_4 aqueous phase (base) in an annular water channel.[75-77] (a) Snapshots of the boat (time interval: 0.1 s). (b) Time-course of θ which is defined in (a).

Such a mode-change in the features of motion is also seen in other chemical reactions, i.e., redox reaction,[78] complex-forming reaction,[79,80] and enzyme reaction.[81] We summarize these reactions and the common and specific points of mode-bifurcation in Table 1. Most systems exhibit a similar mode-change, i.e., continuous → oscillatory → no motion, depending on the concentration of the reactant. However, the formation of a ferroin complex, which is composed of Fe^{2+} and 1,10-phenanthroline, shows a different pattern since ferroin, which consists of three phenanthroline and Fe^{2+}, at higher concentration becomes the driving force of motion.[79,80]

Table 1. Experimental systems for the mode-change in the features of motion depending on the concentration of a reactant coupled with chemical reactions. **C**, **O**, and **N** correspond to continuous, oscillatory, and no motion, respectively.

Reaction	Self-propelled solid object	Reactant in the aqueous phase	Features of motion depending on [reactatnt]	Ref.
acid-base	camphoric acid	HPO_4^{2-} (base)	**C**→**O**→**N**	76, 77
redox	benzoquinone	ascorbic acid or NADPH	**C**→**O**→**N**	78, 81
complex formation	1,10-phenanthroline	Fe^{2+} (metal ion)	**C**→**O**→**C**	79, 80
enzyme	benzoquinone	G6PDH	**C**→**O**→**N**	81

Ikezoe et al. developed a metal–organic framework (MOF) motor with diphenylalanine (DPA) peptides.[82] When DPA peptides are released from MOF to the water surface by the complex formation of an EDTA complex, the surface tension around MOF is decreased, i.e., the driving force of motion is available.

3.2 Photochemical reactions

In this section, we describe how the features of motion change characteristically coupled with photochemical reactions as a noncontact controllable system. First, we describe a benzoquinone (BQ) system. Under ultraviolet (UV) light irradiation, continuous motion and oscillatory motion of a BQ disk change to oscillatory motion and no motion, respectively.[83] The mechanism of this mode-change in the photochemical reaction is similar to that in the redox reaction (see Section 3-1),[78] i.e., hydroquinone (HQ) is produced by the photochemical reaction of BQ under UV light irradiation.[84]

A change in the motion of a droplet can be realized by using azo compounds which exhibit cis-trans photoisomerization under UV or visible light irradiation. Ichimura et al. reported the control of motion of an olive oil droplet on a silica surface modified with an azobenzene derivative.[85] The driving force of motion is the change in the contact angle at the oil/solid interface which is induced by the gradient of light irradiation. Diguet et al. reported the photomanipulation of an oleic acid droplet on an azobenzene trimethylammonium bromide surfactant solution based on the chromocapillary effect, for which driving force is the difference in interfacial tension.[86] Florea reported that a lipophilic droplet on an aqueous solution moves to higher pH induced by the local light stimulation.[87]

As an extension of these studies, the mode-change of a camphor disk can be realized by using 4-[[(dodecyloxy)benz-4-yl]azo]benzoic acid (DBA).[88] The surface pressure of a DBA molecular layer under the UV light irradiation is higher than that under green light irradiation.[89] Therefore, the velocity and features of the self-motion of camphor can be changed by the switching between UV and green light irradiation due to the change in the surface pressure around the camphor disk.[89]

3.3 Design of self-propelled motors based on the molecular structure

In this section, we describe how to design a self-propelled motor that exhibits characteristic features of motion and mode-bifurcation from the viewpoint of the molecular structure. The driving force of self-motion is the surface tension. In other words, the characteristic features of motion are due to the properties of an amphiphilic substance on water, i.e., the characteristic surface pressure (Π) – surface area (A) isotherm which depends on the molecular structure.

For example, the Π–A isotherm for an *N*-stearoyl-*p*-nitroaniline (C_{18}ANA) monolayer has a local minimum and local maximum values, i.e., the system is highly nonlinear.[89-91] By using this property of C_{18}ANA, reciprocating motion can be created even without a physical boundary like a linear water channel, as shown in Fig. 9. The detailed molecular properties of C_{18}ANA and other materials based on a spectroscopic study are described in Section 3.4 and the related papers.[90-92]

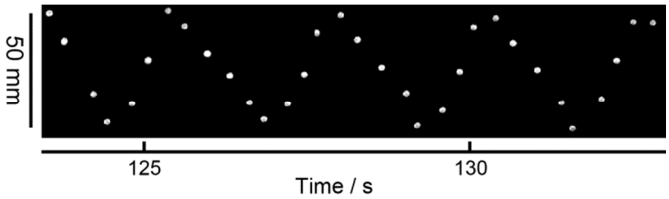

Fig. 9 Time-course of snapshots of a camphor disk on a C_{18}ANA monolayer at 286 K (A = 0.14 nm^2 molecule^{-1}; time interval, 0.3 s).[90-92] The individual snapshots were trimmed in the same space.

In other solid systems, a disk of camphor or its derivative exhibits characteristic motion depending on the structure and concentration of the surfactant in the aqueous phase. Especially, four mode-changes (continuous → oscillatory → continuous → oscillatory → no motion) are generated with an increase in the concentration of soluble anionic surfactant such as SDS. Such a characteristic motion has been discussed in relation to the re-generation of Marangoni flow.[93,94] Toyota and Banno designed self-propelled droplets under nonequilibrium conditions. The features of motion characteristically depend on the properties and chemical reactions (e.g., hydrolysis) of synthesized surfactants.[95,96]

4. Characterization of adsorbed molecules on water

This chapter describes analytical techniques that are useful for characterizing molecules adsorbed at an air/water interface. For the analysis of motion of an object on water, the observation of monolayer domains of the adsorbed molecules and a spectroscopic understanding of the monolayer are both necessary.

A Brewster angle microscope (BAM)[97] is a powerful tool for monitoring the motion of a floating object in an opening between monolayer domains. The p-polarized ray that shows electric-field oscillation parallel to the incident plane[98] is known to have a unique property: reflectance at an interface becomes zero at a specific angle of incidence, Brewster's angle, θ_B,[98] which is defined as:

$$\theta_B = \tan^{-1}(n_2/n_1) \quad (5)$$

where n_1 and n_2 are the refractive indices of the two phases separated at the interface ($n_1 < n_2$). In most cases, n_1 corresponds to the air phase. Therefore, when a p-polarized ray is irradiated at the air ($n_1 = 1.0$)/water ($n_2 = 1.33$) interface, θ_B becomes 53° from the surface normal. If a monolayer ($n \approx 1.5$) is floating on water, θ_B changes on the monolayer because of the different refractive index. When the reflected ray is led to a camera, the monolayer domains and the remaining bare water surfaces yield an image by the optical contrast. In this manner, the ultrathin monolayer domains can be visualized.

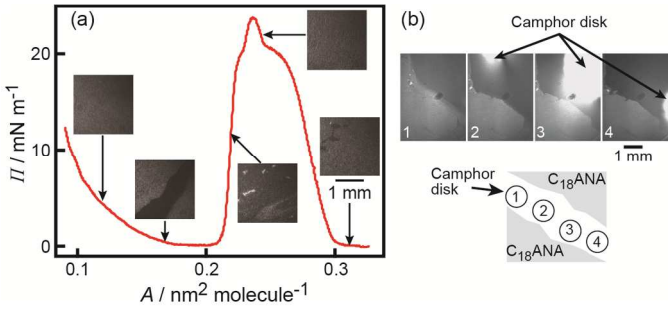

Fig. 10 (a) BAM images of a C_{18}ANA monolayer at various surface areas and the simultaneously measured *Π-A* isotherm of the C_{18}ANA monolayer on water.[92] (b) Snapshots of a BAM image when a camphor disk reciprocated on a C_{18}ANA monolayer (A = 0.2 nm molecules^{-1}). The temperature of the aqueous phase was 298 K. Reprinted with permission from [92]. Copyright 2014 American Chemical Society.

Figure 10a presents BAM images of a C_{18}ANA monolayer on water during monolayer compression along with the *Π-A* isotherm.[92] At a large surface area of ca. 0.3 nm^2 molecule^{-1}, bright dots and dark areas, which correspond to molecular aggregates of C_{18}ANA and the bare water surface, respectively, are observed. On compression, the dark parts disappear, and a homogeneous monolayer is formed (A = 0.24 nm molecule^{-1}), which corresponds to an increase in the surface pressure in the *Π-A* isotherm.

When the monolayer is further compressed, however, molecular fastening due to intermolecular hydrogen bonding on the amide group occurs, which results in a rapid decrease in the surface pressure. In this region (A = 0.17 nm molecule^{-1}), the BAM image shows highly homogeneous domains and water surface. In this manner, the discussion of the *Π-A* isotherm can strongly be supported by the BAM analysis. Figure 10b suggests that reciprocating motion of a camphor disk is generated on pure water and the trajectory of reciprocation is maintained because of the irreversible condensation of the C_{18}ANA molecular layer.

IR spectroscopic analysis of the monolayer on water is another powerful tool. Since water vapour strongly interferes with IR measurements, the IR analysis of a monolayer on water is generally quite difficult. Since the reflectance on water is very low due to the low refractive index of water,[98] we have another difficulty of poor throughput for reflection measurements. Here, a representative technique of polarization modulation infrared reflection-absorption spectrometry (PM-IRRAS)[99,100] is introduced to overcome these difficulties.

PM-IRRAS (Fig. 11) uses a photoelastic modulator (PEM) to drive IR polarization at a high speed such as 5 kHz. When the PEM is operated electrically with a modulation frequency of ω_m, the intensity, I, of the linearly polarized IR ray by the $\lambda/2$ waveplane is modulated as:[99]

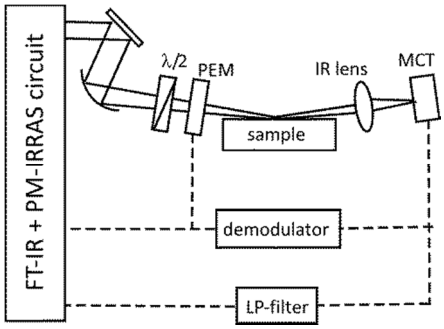

Fig. 11 Schematic diagram of PM-IRRAS in FT-IR. The solid and dashed lines represent light and electric signal paths, respectively.

$$I = \frac{I_0}{2}\left[R_s + R_p + J_0(\phi_0)\left(R_p - R_s\right)\right] - \frac{I_0}{2}\left[J_2(\phi_0)\cos(2\omega_m t)\left(R_p - R_s\right)\right] \quad (6)$$

Here, R_s and R_p are reflectance at the sample surface for s- and p-polarizations, respectively, and the difference in the polarization response on the detector is omitted for simplicity. J_0 and J_2 are Bessel's functions, and ϕ_0 is the initial phase determined by PEM and the wavenumber of the IR ray. In practice, linear and circular polarized IR rays are generated rapidly. Since only the latter term is a function of time, the former and latter terms are called the DC and AC terms, respectively. Only the DC term is separated by passing the signal to a low-pass (LP) filter when ω_m is adequately larger than the modulation frequency of the FT-IR. On the other hand, the AC term is obtained by using a 'demodulator', which removes the $\cos(2\omega_m t)$ term. As a result, the spectrometer receives the two signals, I_{DC} and I_{AC}, simultaneously.

Here, the ratio spectrum, S, is defined as:

$$S \equiv \frac{I_{AC}}{I_{DC}} = \left|\frac{J_2(\varphi_0)\left(R_p - R_s\right)}{R_p + R_s + J_0(\varphi_0)\left(R_p - R_s\right)}\right| \quad (7)$$

When the substrate, on which a monolayer is deposited, is a dielectric (non-metallic) material, the ratio spectrum is difficult to simplify further. In this case, the normalized ratio spectrum is convenient for discussing the spectrum.

$$\frac{\Delta S}{S(0)} = \frac{S(d) - S(0)}{S(0)} \quad (8)$$

Here, $S(d)$ and $S(0)$ are the ratio spectra of the sample and background measurements, respectively.

In general, PM-IRRAS measurements are performed with an angle of incidence of 76°.[99,101] When the normalized ratio spectrum intensity is calculated as a function of the orientation, the surface selection rule of PM-IRRAS is obtained, which should be quite useful for discussing the spectra.[102,103]

Figure 12 shows PM-IRRAS spectra of monolayers of fatty acids of different chain lengths on water.[102] The band positions of the CH_2 stretching vibration bands respond to the molecular

conformation. For example, the anti-symmetric stretching vibration ($\nu_a(CH_2)$) band appears at 2916 cm^{-1} when the chain is highly ordered; whereas it is shifted to a higher wavenumber position for a disordered chain. The monolayer of nonadecanoic acid is thus found to be highly stabilized even at a low surface pressure of 2 mN m^{-1}, while the stability is lost for a short fatty acid, and no even-odd effect is found.

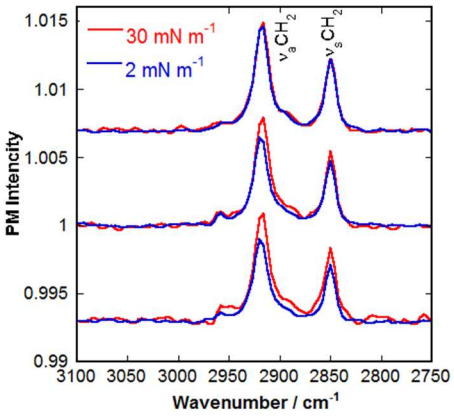

Fig.12 PM-IRRAS spectra of monolayers of (a) heptadecanoic acid, (b) octadecanoic acid, and (c) nonadecanoic acid on water. The blue and red spectra are measured at 2 and 30 mN m^{-1}, respectively.

Judging from the surface selection rule, the positive peaks indicate that both CH_2 anti-symmetric and symmetric stretching vibration bands are nearly parallel to the water surface, which results in a nearly perpendicular orientation of the hydrocarbon axis to the surface.

5. Mathematical modelling

A mathematical model can be used to not only clarify the mechanism of the characteristic features of motion but also to design a novel self-propelled system. This chapter describes how the spatio-temporal features of self-motion can be reproduced by a mathematical model that is composed of the reaction-diffusion equation and equations of motion.[19,21] The mathematical model of this chapter unifies various mathematical models suggested in previous researches.

5.1 Mathematical model for the self-motion of a camphor disk on water

For the one-dimensional motion of a camphor disk on the x-axis, the reaction-diffusion equation is expressed as

$$\frac{\partial u}{\partial t} = D\frac{\partial^2 u}{\partial x^2} - ku + F(x, x_c; r), \tag{9}$$

where u is the surface concentration of camphor molecules on water, k is the rate constant of the sum of the sublimation and dissolution of developed camphor molecules, x_c is the central coordinate of the camphor disk, r is the radius of the camphor disk, and F is the development of camphor molecules from the solid camphor to the water.

The equation of motion is

$$\rho\ddot{x}_c = \frac{\gamma(u(t, x_c + r)) - \gamma(u(t, x_c - r))}{2r} - \mu\dot{x}_c, \tag{10}$$

where ρ, γ, and μ are the mass density, surface tension, and the constant of viscosity, respectively. For the driving force of motion, the surface tension, $\gamma(u)$, is expressed as eqn (4).

$F(x, x_c, r)$ is given as

$$F(x, x_c, r) = \begin{cases} S_0, |x - x_c| \le r, \\ 0, |x - x_c| > r. \end{cases} \tag{11}$$

The self-motion of a camphor disk can be qualitatively reproduced based on eqns (4), (9)-(11).[21] Actual parameters were estimated experimentally.[37]

5.2 Mathematical model for synchronized swimming

Next, we describe the self-motion of two equivalent boats (α, β) on an annular water channel.[34] Here, we introduce model equations for the two camphor boats to reproduce phase-locking and phase-oscillatory synchronization. We approximate a camphor boat as two rigid material particles:

$$x_1(t) = x_c(t) + l, x_2(t) = x_c(t) - l \tag{12}$$

where x_1 denotes the front of the camphor boat, x_2 is the rear, and $2l$ is the length of the camphor boat. The reaction-diffusion equation of the molecular layer of camphor is

$$\frac{\partial u}{\partial t} = D\frac{\partial^2 u}{\partial x^2} - ku + \sum_{i=\alpha,\beta} F(x, x_2^i; r), \tag{13}$$

The Newtonian equation of motion for one boat α or β can be expressed as

$$\rho\ddot{x}_c^i = \frac{\gamma(u(t, x_1^i)) - \gamma(u(t, x_2^i))}{2l} - \mu\dot{x}_c^i, \tag{14}$$

where i denotes the camphor boat, α or β. As a boundary condition of eqn (6), we take the following periodic boundary conditions:

$$u(t,0) = u(t.L), \frac{\partial}{\partial x}u(t,0) = \frac{\partial}{\partial x}u(t, L), \tag{15}$$

where L is the length of the circular water channel. Figure 13 shows the numerical results for the time-course of the phase difference between two camphor boats, $\Delta\theta$, based on eqns (12)-(15). The phase-locking (Fig.13a) and phase-oscillatory (Fig.13b) synchronization in the experiments[34] are well reproduced theoretically depending on the coefficient, k.

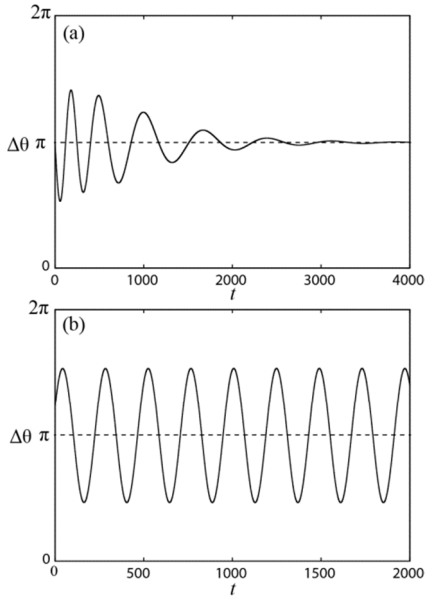

Fig.13 Numerical results on the time-course of the phase difference between two equivalent camphor boats, $\Delta\theta$, for k = (a) 0.5 and (b) 1.0 based on eqns (12)-(15).[34] The parameters are D = 2.0, S_0 = 1.0, μ = 0.035, γ_0 = 1.0, γ_1 = 0.0, p = 2, a = 0.01, l = 0.5, r = 0.5, L = 16.

5.3 Mathematical model for self-motion coupled with a chemical reaction

Next, we describe a mathematical model for the self-motion of camphor derivatives, such as camphoric acid, coupled with a chemical reaction. We consider a numerical model of the acid-base reaction between camphoric acid and Na_2HPO_4 (see Section 3.1) is described in eqn (16):[74]

$$m(\mathrm{H}_n\mathrm{A}) + n\mathrm{B} \xrightarrow{k_r} m\mathrm{A}^{n-} + n(\mathrm{H}_m\mathrm{B})^{m+}, \tag{16}$$

where H_nA and B are acid and base. H_nA is ionized to A^{n-} around the air-water interface. The reaction-diffusion equations for H_nA and B are shown in eqn (17).

$$\begin{cases} \dfrac{\partial u}{\partial x} = D_u \dfrac{\partial^2 u}{\partial x^2} - k_d u - m k_r u^m v^n + F\left(x, x_2(t); r_0\right) \\ \dfrac{\partial v}{\partial x} = D_v \dfrac{\partial^2 v}{\partial x^2} - n k_r u^m v^n \end{cases}, \tag{17}$$

As the boundary condition, we take the following non-flux condition

$$\frac{\partial}{\partial x}u(t,0) = \frac{\partial}{\partial x}u(t,L), \frac{\partial}{\partial x}v(t,0) = \frac{\partial}{\partial x}v(t,L) \tag{18}$$

The Newtonian motion of equation for one boat can be expressed as

$$\rho\ddot{x}_c = \frac{\gamma\left(u(t,x_1)\right) - \gamma\left(u(t,x_2)\right)}{2l} - \mu\dot{x}_c. \tag{19}$$

To investigate the dependence of the concentration of B, we use the following initial conditions:

$$\begin{aligned} u(0,x) = 0, v(0,x) = v_0 \\ x_c(0) = x_a, \dot{x}_c = 0, \end{aligned} \tag{20}$$

where v_0 is the initial concentration of B. We can perform our numerical simulation based on eqns (17)-(20). We assume that D_v/D_u is very small since the surface diffusion of the organic acid layer is significantly greater than the diffusion of the base ion in the bulk phase. Figure 14 shows the numerical results for the self-motion of an organic acid boat depending on v_0 based on eqns (18)-(21) in the case of m =1 and n = 2, i.e., the case of camphoric acid. When v_0 is small, the boat exhibits uniform motion (Fig.14a) and the velocity decreases with an increase in v_0.[79] When v_0 is mid-range, uniform motion changes to oscillatory motion (Fig.14b), and the period of oscillation increases with an increase in v_0 (Fig.14c). These results suggest that the boat changes from uniform motion to oscillatory motion by Hopf bifurcation with an increase in v_0. Finally, we numerically confirm that the mode-change depends on the reaction order m and n. If $m \geq n$, oscillatory motion does not occur. This result suggests that the reaction order is important for reproducing oscillatory motion.[79]

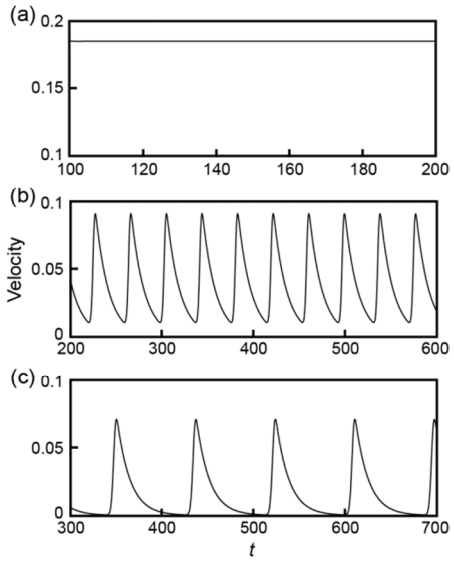

Fig.14 Numerical results for the time-course of the velocity of x_c at v_0 = (a) 10.0, (b) 50, and (c) 140 based on eqns (17)-(20).[77] The parameters are D_u = 1.0, D_v = 0.00001, k_d = 1.0, k_r = 1.0, m = 1, n =2, ρ = 1.0, S_0 = 1.0, μ = 0.07, γ_0 = 10.0, γ_1 = 0.0, a = 0.3, p = 4, l = 1.0, r = 0.5, L = 40.

6. Conclusions and outlook

Self-propelled motors, which, like living organisms, exhibit characteristic features of motion at interfaces depending on the physicochemical environment, can be realized artificially from the viewpoint of nonlinear phenomena. Mathematical

modelling based on the experimental results for non-living motors is also important for not only understanding but also confirming the mechanism of characteristic motion in both non-living and living systems. In addition, the synthesis of compounds that exhibit nonlinearity, such as C_{18}ANA, and their spectroscopic analysis are also significant for considering the relationship between self-motion and nonlinearity from the viewpoint of the molecular structure. With regard to collective motion, a single self-propelled motor will exhibit monotonic motion or irregular motion. However, we cannot image collective motion using only a single motor since collective motion can only be produced by the interaction between multiple motors.

For the design of intelligent non-living self-propelled motors that mimic biological motors, the development of individual parts that have specific functions is important. In addition, the present perspective suggests that the interaction between self-propelled motors and reaction-diffusion-convection dynamics is also important for enhancing the features of motion, since the characteristic features of motion, like a dynamic pattern formation, can be spontaneously reproduced even if they are disturbed by an external perturbation.

Acknowledgements

We thank Mr. Tomoaki Ueda, Mr. Yui Matsuda, Ms. Miyu Yoshii, Ms. Sena Mizumoto (Hiroshima University, Japan), and Prof. Takafumi Shimoaka (Kyoto University, Japan) for their technical assistance. We thank Prof. Kenichi Yoshikawa (Doshisha University, Japan) and Prof. Toshio Ishii for their fruitful discussion. This work was supported in part by a Grant-in-Aid for Scientific Research (No. 25410094), the Sekisui Chemical Grant Program for Research on Manufacturing Based on Innovations Inspired by Nature to SN, and Platform for Dynamic Approaches to Living System from the Ministry of Education, Culture, Sports, Science and Technology, Japan. This work was also performed under the Cooperative Research of "Network Joint Research Center for Materials and Devices".

Notes

[a] *Graduate School of Science, Hiroshima University, 1-3-1 Kagamiyama, Higashi-Hiroshima 739-8526, Japan. E-mail: nakatas@hiroshima-u.ac.jp*

[b] *Research Institute for Electronic Science, Hokkaido University, N20W10, Kita-Ward, Sapporo, 001-0020, Japan. E-mail: nagayama@es.hokudai.ac.jp*

[c] *CREST, Japan Science and Technology Agency, Tokyo, Japan.*

[d] *Department of Physics, Graduate School of Science, Chiba University, 1-33, Yayoi-cho, Inage-ku, Chiba 263-8522, Japan. E-mail: kitahata@chiba-u.jp*

[e] *Graduate School of Advanced Mathematical Sciences, Meiji University, 4-21-1 Nakano, Tokyo 164-8525, Japan. E-mail: suematsu@meiji.ac.jp*

[f] *Meiji Institute of Advanced Study of Mathematical Sciences, Meiji University, 4-21-1 Nakano, Tokyo 164-8525, Japan.*

[g] *Institute for Chemical Research, Kyoto University, Uji, Kyoto 611-0011, Japan. E-mail: htakeshi@scl.kyoto-u.ac.jp*

References

1 S. J. Ebbens and J. R. Howse, *Soft Matter*, 2010, **6**, 726–738.
2 Y. Hong, D. Velegol, N. Chaturvedic and A. Sen, *Phys. Chem. Chem. Phys*., 2010, **12**, 1423–1435.
3 W. F. Paxton, S. Sundararajan, T. E. Mallouk and A. Sen, *Angew. Chem. Int. Ed.*, 2006, **45**, 5420–5429.
4 C. D. Bain, G. D. Burnett-Hall and R. R. Montgomerie, *Nature*, 1994, **372**, 414–415.
5 M. K. Chaudhury and G. M. Whitesides, *Science*, 1992, **256**, 1539–1541.
6 P. G. de Gennes, *Physica A*, 1998, **249**, 196–205.
7 J. Bico and D. Quéré, *J. Fluid Mech.*, 2002, **467**, 101–127.
8 V. Pimienta and C. Antoine, *Curr. Opin. Colloid Interface Sci.*, 2014, **19**, 290–299.
9 P.-G. de Gennes, F. Brochard and D. Quere, *Capillarity and Wetting Phenomena: Drops, Bubbles, Pearls, Waves*, Springer, 2004.
10 C. Tomlinson, *Proc. R. Soc. London*, 1860, **11**, 575–577.
11 L. Rayleigh, *Proc. R. Soc. London*, 1890, **47**, 364–367.
12 L. Zhang, J. J. Abbott, L. Dong, B. E. Kratochvill, D. Bell and B. J. Nelson, *Appl. Phys. Lett.,* 2009, **94**, 064107.
13 O. D.Velev, B. G. Prevo and K. H. Bhatt, *Nature*, **426**, 2003, 515–516.
14 H. C. Berg, *Annu. Rev. Biochem.*, 2003, **72**, 19–54.
15 R. Kapral and K. Showalter, *Chemical Waves and Patterns*, Kluwer Academic, Dordrecht, 1994.
16 A T. Winfree, *The Geometry of Biological Time*, Springer, Berlin, 2001.
17 Y. Kuramoto, *Chemical Oscillations, Waves, and Turbulence*, Springer, New York, 1984.
18 S. Nakata, Y. Iguchi, S. Ose, M. Kuboyama, T. Ishii and K. Yoshikawa, *Langmuir*, 1997, **13**, 4454–4458.
19 M. Nagayama, S. Nakata, Y. Doi and Y. Hayashima, *Physica D*, 2014, **194**, 151–165.
20 N. Bassik, B. T. Abebe and D. H. Gracias, *Langmuir*, 2008, **24**, 12158-12163.
21 Y. Hayashima, M. Nagayama and S. Nakata, *J. Phys. Chem. B*, 2001, **105**, 5353–5357.
22 S. Nakata, Y. Hayashima and H. Komoto, *Phys. Chem. Chem. Phys*., 2000, **2**, 2395–2399.
23 S. Nakata and S. Hiromatsu, *Colloids Surf. A*, 2003, **224**, 157–163.
24 N. J. Suematsu, Y. Ikura, M. Nagayama, H. Kitahata, N. Kawagishi, M. Murakami and S. Nakata, *J. Phys. Chem. C*, 2010, **114**, 9876–9882.
25 R. Sharma, S. T. Chang and O. D. Velev, *Langmui*r, 2012, **28**, 10128−10135.
26 V. I. Kovalchuk, H. Kamusewitz, D. Vollhardt and N. M. Kovalchuk, *Phys. Rev. E*, 1999, **60**, 2029−2036.
27 S. Nakata, M. Hata, Y. S. Ikura, E. Heisler, A. Awazu, H. Kitahata and H. Nishimori, *J. Phys. Chem. C*, 2013, **117**, 24490−24495.
28 D. dos Santos and T. Ondarçuhu, *Phys. Rev. Lett.*, 1995, **75**, 2972−2975.
29 T. Ohta and T. Ohkuma, *Phys. Rev. Lett.*, 2009, **102**, 154101.

30 H. Kitahata, K. Iida, and M. Nagayama, *Phys. Rev. E*, 2013, **87**, 010901.
31 K. Iida, H. Kitahata, and M. Nagayama, *Physica D*, 2014, **272**, 39-50.
32 A. Pikovsky, M. Rosenblum and J. Kurths, *Synchronization: A Universal Concept on Nonlinear Sciences;* Cambridge University Press: Cambridge, 2001.
33. T. Vicsek and A. Zafeiris, *Phys. Rep.*, 2012, **517**, 71-140.
34 M. I. Kohira, Y. Hayashima, M. Nagayama and S. Nakata, *Langmuir*, 2001, **17**, 7124–7129.
35 N. J. Suematsu, T. Sasaki, S. Nakata and H. Kitahata, *Langmuir*, 2014, **30**, 8101–8108.
36 S. Nakata, M. I. Kohira and Y. Hayashima, *Chem. Phys. Lett.*, 2000, **322**, 419–423.
37 S. Nakata, Y. Doi and H. Kitahata, *J. Phys. Chem. B*, 2005, **109**, 1798–1802.
38 N. J. Suematsu, S. Nakata, A. Awazu and H. Nishimori, *Phys Rev. E*, 2010, **81**, 056210.
39 Y. Sugiyama, M. Fukui, M. Kikuchi, K. Hasebe, A. Nakayama, K. Nishinari, S. Tadaki, and S. Yukawa, *New J. Phys.*, 2008, **10**, 033001.
40 M. Bando, K. Hasebe, A. Nakayama, A. Shibata and Y. Sugiyama, *Phys. Rev. E*, 1995, **51**, 1035.
41 E. Heisler, N. J. Suematsu, A. Awazu and H. Nishimori, *Phys. Rev. E*, 2012, **85**, 055201(R).
42 E. Heisler, N. J. Suematsu, A. Awazu and H. Nishimori, *J. Phys. Soc. Jpn.*, 2012, **81**, 074605.
43 Y. S. Ikura, E. Heisler, A. Awazu, H. Nishimori and S. Nakata, *Phys. Rev. E*, 2013, **88**, 012911.
44 S. Soh, K. J. M. Bishop and B. A. Grzybowski, *J. Phys. Chem. B*, 2008, **112**, 10848–10853.
45 S. Soh, M. Branicki and B. A. Grzybowski, *J. Phys. Chem. Lett.*, 2011, **2**, 770–774.
46 N. J. Suematsu, K. Tateno, S. Nakata and H. Nishimori, *J. Phys. Soc. Jpn.*, in press.
47 O. Schulz and M. Markus, *J. Phys. Chem. B*, 2007, **111**, 8175–8178.
48 T. Bánsági Jr., M. M. Wrobel, S. K. Scott and A. F. Taylor, *J. Phys. Chem. B*, 2013, **117**, 13572−13577.
49 L. E. Scriven and C. V. Sternling, *Nature*, 1960, **187**, 186–188.
50 H. Kitahata, S. Hiromatsu, Y. Doi, S. Nakata and M. R. Islam, *Phys. Chem. Chem. Phys.*, 2004, **6**, 2409–2414.
51 Y. S. Ikura, R. Tenno, H. Kitahata, N. J. Suematsu and S. Nakata, *J. Phys. Chem. B*, 2012, **116**, 992–996.
52 S. Nakata, R. Tenno, A. Deguchi, H. Yamamoto, Y. Hiraga and S. Izumi, *Colloids Surf. A*, 2015, **466**, 40–44.
53 H. Kitahata, K. Kawata, Y. Sumino and S. Nakata, *Chem. Phys. Lett.*, 2008, **457**, 254–258.
54 H. Kitahata, K. Kawata, S. Takahashi, M. Nakamura, Y. Sumino and S. Nakata, *J. Colloid Interface Sci.*, 2010, **351**, 299–303.
55 S. Nakata, Y. Doi and H. Kitahata, *J. Colloid Interface Sci.*, 2004, **279**, 503–508.
56 H. Kitahata, R. Aihara, N. Magome and K. Yoshikawa, *J. Chem. Phys.*, 2002, **116**, 5666-5672.
57 H. Kitahata, N. Yoshinaga, K. H. Nagai and Y. Sumino, *Chem. Lett.*, 2012, **41**, 1052-1054.
58 H. Kitahata, N. Yoshinaga, K. H. Nagai and Y. Sumino, *Phys. Rev. E*, 2011, **84**, 015101.
59 J. Szymanski, J. Gorecki and M. J. B. Hauser, *J. Phys. Chem. C*, 2013, **117**, 13080−13086.
60 D. Taniguchi, S. Ishihara, T. Oonuki, M. Honda-Kitahara, K. Kaneko and S. Sawai, *Proc. Natl. Acad. Sci.*, 2013, **110**, 5016−5021.
61 M. Dupayrat and E. Nakache, *Bioelectrochem. Bioenerg.*, 1978, **5**, 134−141.
62 K. Yoshikawa and Y. Matsubara, *J. Am. Chem. Soc.*, 1983, **105**, 5967−5969.
63 K. Yoshikawa, M. Shoji, S. Nakata, S. Maeda and H. Kawakami, *Langmuir*, 1988, **4**, 759−762.
64 N. Magome and K. Yoshikawa, *J. Phys. Chem.*, 1996, **100**, 19102−19105.
65 S. Matsushita, S. Tanaka, K. Yoshida, K. Kobayashi, Y. Tsuruki, Y. Shibuya, T. Isobe and A. Nakajima, *Colloids Surf. A*, 2012, **395**, 233–239.
66 A. Shioi, K. Katano, and Y. Onodera, *J. Colloid Interface Sci.*, 2003, **266**, 415–421.
67 Y. Sumino, N. Magome, T. Hamada and K. Yoshikawa, *Phys. Rev. Lett.*, 2005, **94**, 068301.
68 B. Nanzai, R. Ishikawa and M. Igawa, *Chem. Lett.*, 2012, **41**, 609−611.
69 S. Nakata and K. Matsuo, *Langmuir*, 2005, **21**, 982–984.
70 O. Sano, K. Kutsumi and N. Watanabe, *J. Phys. Chem. Jpn.*, 1995, **64**, 193–1999.
71 S. Nakata, H. Komoto, K. Hayashi and M. Menzinger, *J. Phys. Chem. B*, 2000, **104**, 3589–3593.
72 T. Ban, K. Tani, H. Nakata and Y. Okano, *Soft Matter*, 2014, **10**, 6316–6320.
73 J. Čejková, M. Novák, F. Štěpánek and M. M. Hanczyc, *Langmuir*, 2014, **30**, 11937–11944.
74 I. Lagzi, S. Soh, P. J. Wesson, K. P. Browne and B. A. Grzybowski, *J. Am. Chem. Soc.*, 2010, **132**, 1198–1199.
75 S. Nakata, Y. Iguchi, S. Ose and T. Ishii, *J. Phys. Chem. B*, 1998, **102**, 7425-7427.
76 Y. Hayashima, M. Nagayama, Y. Doi, S. Nakata, M. Kimura and M. Iida, *Phys. Chem. Chem. Phys.*, 2002, **4**, 1386–1392.
77 M. Nagayama, M. Yadome, M. Murakami, N. Kato, J. Kirisaka and S. Nakata, *Phys. Chem. Chem. Phys.*, 2009, **11**, 1085–1090.
78 N. J. Suematsu, Y. Miyahara, Y. Matsuda and S. Nakata, *J. Phys. Chem. C*, 2010, **114**, 13340–13343.
79 S. Nakata and Y. Arima, *Colloids Surf. A*, 2012, **324**, 222–227.
80 K. Iida, N. J. Suematsu, Y. Miyahara, H. Kitahata, M. Nagayama and S. Nakata, *Phys. Chem. Chem. Phys.*, 2010, **12**, 1557–1563.
81 S. Nakata, Y. Matsuda, Y. S. Ikura, A. Takeda and S. Izumi, *ChemPhysChem*, 2012, **13**, 520–524.
82 Y. Ikezoe, G.Washino, T. Uemura, S. Kitagawa and H. Matsui, *Nature Mater.*, 2012, **11**, 1081–1085.
83 Y. Matsuda, N. J. Suematsu and S. Nakata, *Phys. Chem. Chem. Phys.*, 2012, **14**, 5988–5991.
84 A. Pochon, P. P. Vaughan, D. Gan, P. Vath, N. V. Blough and D. E. Falvey, *J. Phys. Chem. A*, 2002, **106**, 2889–2894.
85 K. Ichimura, S.-K. Oh and M. Nakagawa, *Science*, 2000, **288**, 1624–1626.
86 A. Diguet, R. -M. Guillermic, N. Magome, A. Saint-Jalmes, Y. Chen, K. Yoshikawa and D. Baigl, *Angew. Chem. Int. Ed.*, 2009, **48**, 9281–9284.

87 L. Florea, K. Wagner, P. Wagner, G. G. Wallace, F. Benito-Lopez, D. L. Officer, D. Diamond, *Adv. Mater.*, 2014, **26**, 7339−7345.
88 F. Vera, J. Barberá, P. Romero, J. L. Serrano, M. B. Ros and T. Sierra, *Angew. Chem., Int. Ed.*, 2010, **49**, 4910−4914.
89 S. Nakata, T. Miyaji, Y. Matsuda, M. Yoshii and M. Abe, *Langmuir*, 2014, **30**, 7353−7357.
90 S. Nakata, T. Miyaji, T. Sato, M. Hoshikawa, Y. S. Ikura and S. Izumi, *ChemPhysChem*, 2012, **13**, 4129−4133.
91 S. Nakata, T. Miyaji, T. Ueda, T. Sato, Y. S. Ikura, S. Izumi and M. Nagayama, *J. Phys. Chem. C*, 2013, **117**, 6346−6352.
92 S. Nakata, T. Ueda, T. Miyaji, Y. Matsuda, Y. Katsumoto, H. Kitahata, T. Shimoaka and T. Hasegawa, *J. Phys. Chem. C*, 2014, **118**, 14888−14893.
93 S. Nakata, J. Kirisaka, Y. Arima and T. Ishii, *J. Phys. Chem. B*, 2006, **110**, 21131−21134.
94 S. Nakata and M. Murakami, *Langmuir*, 2010, **26**, 2414−2417.
95 T. Toyota, N. Maru, M. M. Hanczyc, T. Ikegami and T. Sugawara, *J. Am. Chem. Soc*., 2009, **131**, 5012–5013.
96 T. Banno, R. Kuroha and T. Toyota, *Langmuir*, 2012, 28, 1190–1195.
97 D. Hoenig and D. Moebius, *J. Phys. Chem*., 1991, **95**, 4590–4592.
98 E. Hecht, *"Optics (2nd ed.)"*, Addison-Wesley, Reading, 1990.
99 D. Blaudez, J. M. Turlet, J. Dufourcq, D. Bard, T. Buffeteau and B. Desbat, *J. Chem. Soc., Faraday Trans.*, 1996, **92**, 525–530.
100 D. Blaudez, T. Buffeteau, J. C. Cornut, B. Desbat, N. Escafre, M. Pezolet and J. M. Turlet, *Appl. Spectrosc.*, 1993, **47**, 869–874.
101 Y. Itoh, M. Muro and T. Hasegawa, *Appl. Spectrosc*., 2010, **64**, 1374–1378.
102 M. Muro, Y. Itoh and T. Hasegawa, *J. Phys. Chem. B*, 2010, **114**, 11496–1150.
103 M. Muro, M. Harada, T. Okada and T. Hasegawa, *J. Phys. Chem. B*, 2012, **116**, 3148–3154.

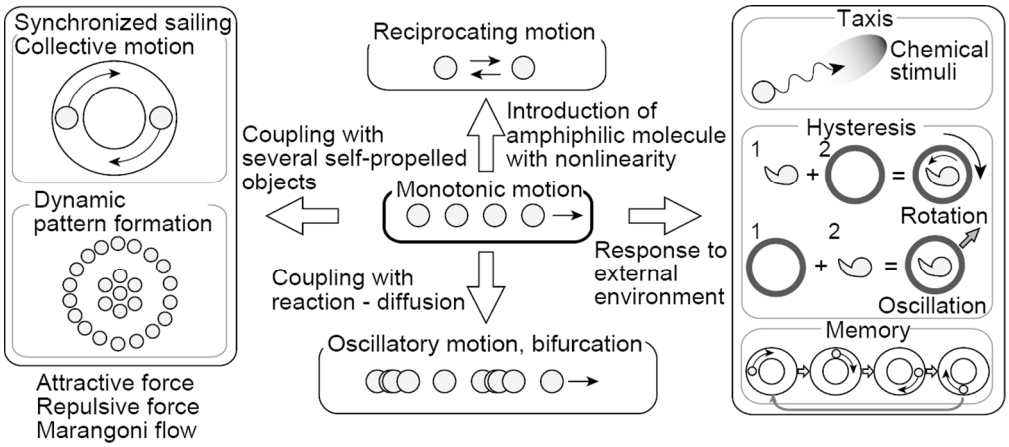

223x98mm (150 x 150 DPI)

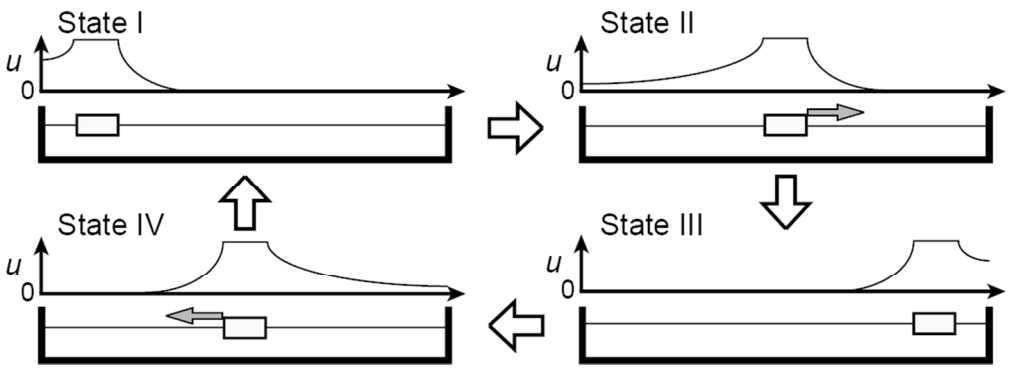

187x67mm (150 x 150 DPI)

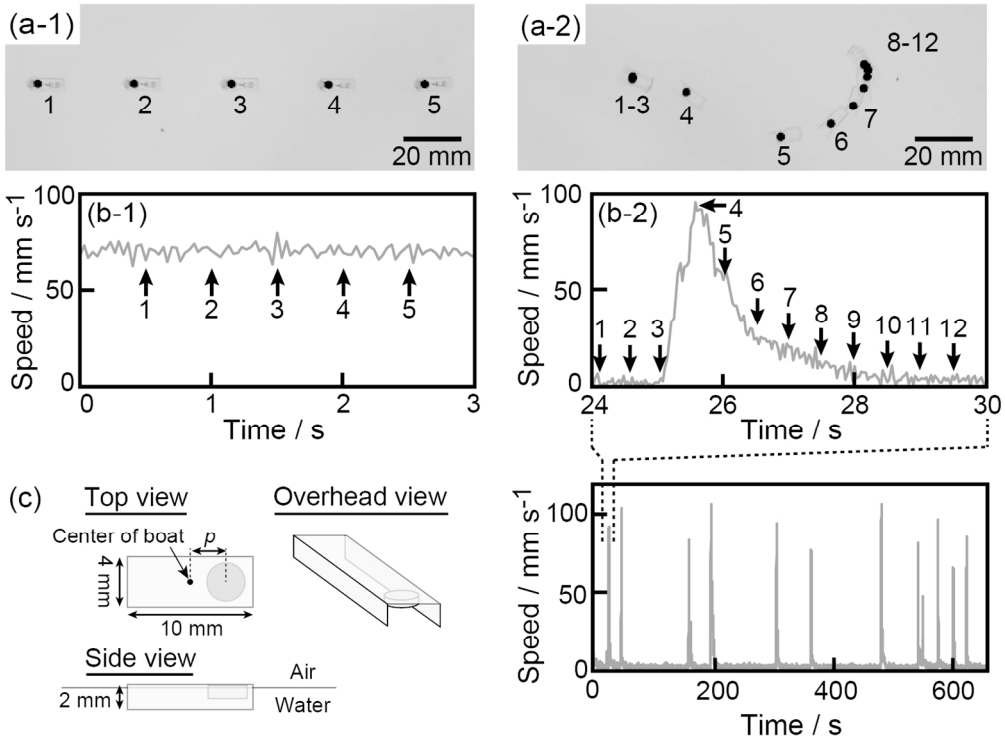

271x200mm (150 x 150 DPI)

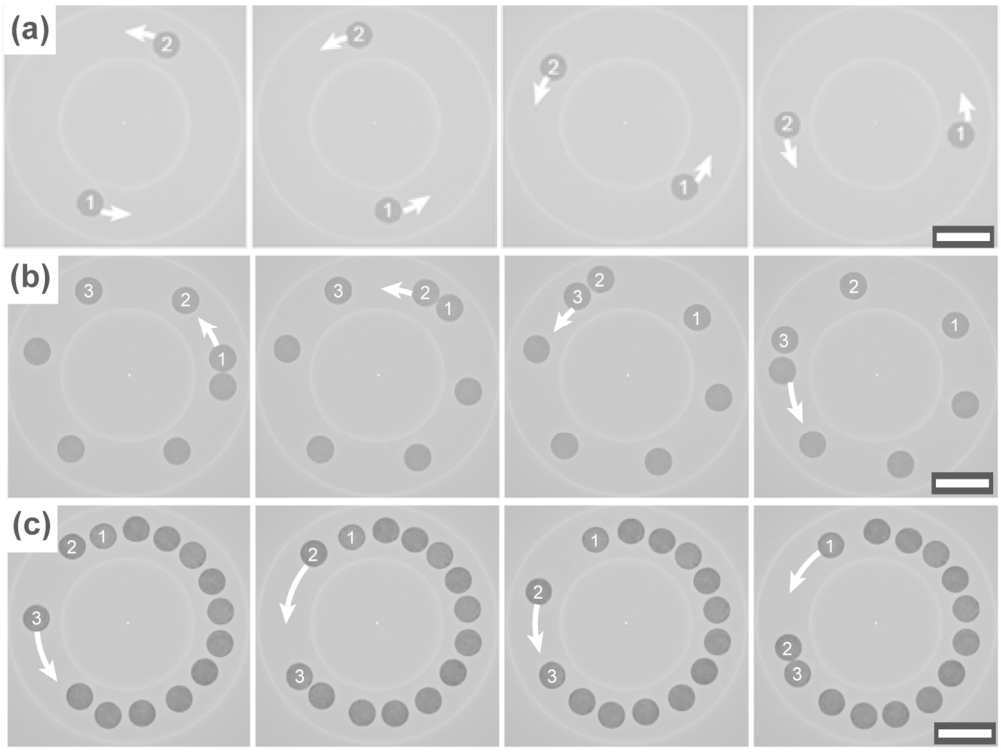

131x98mm (300 x 300 DPI)

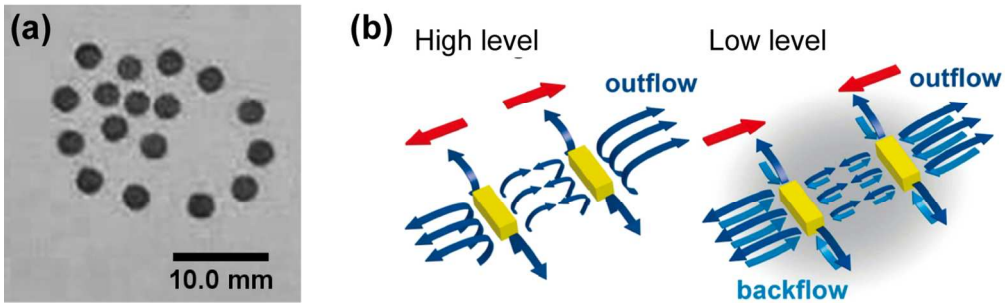

124x37mm (300 x 300 DPI)

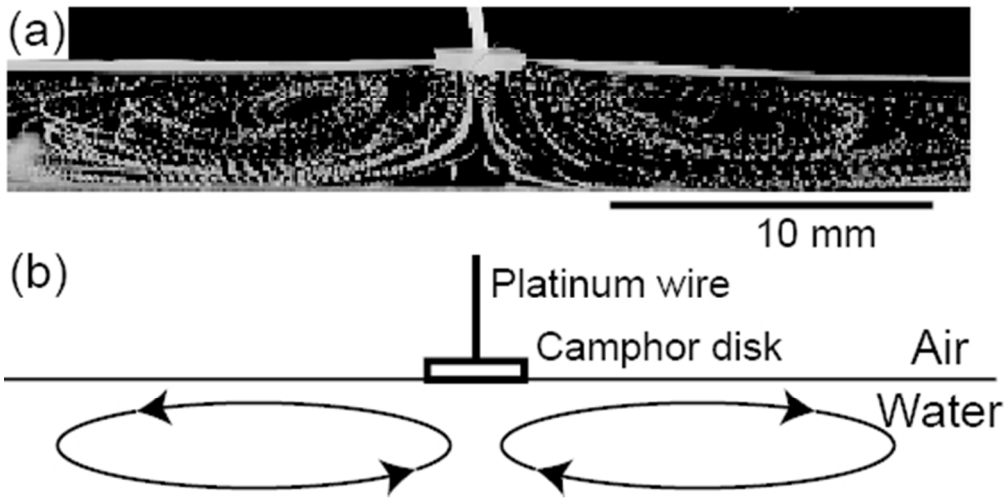

88x44mm (150 x 150 DPI)

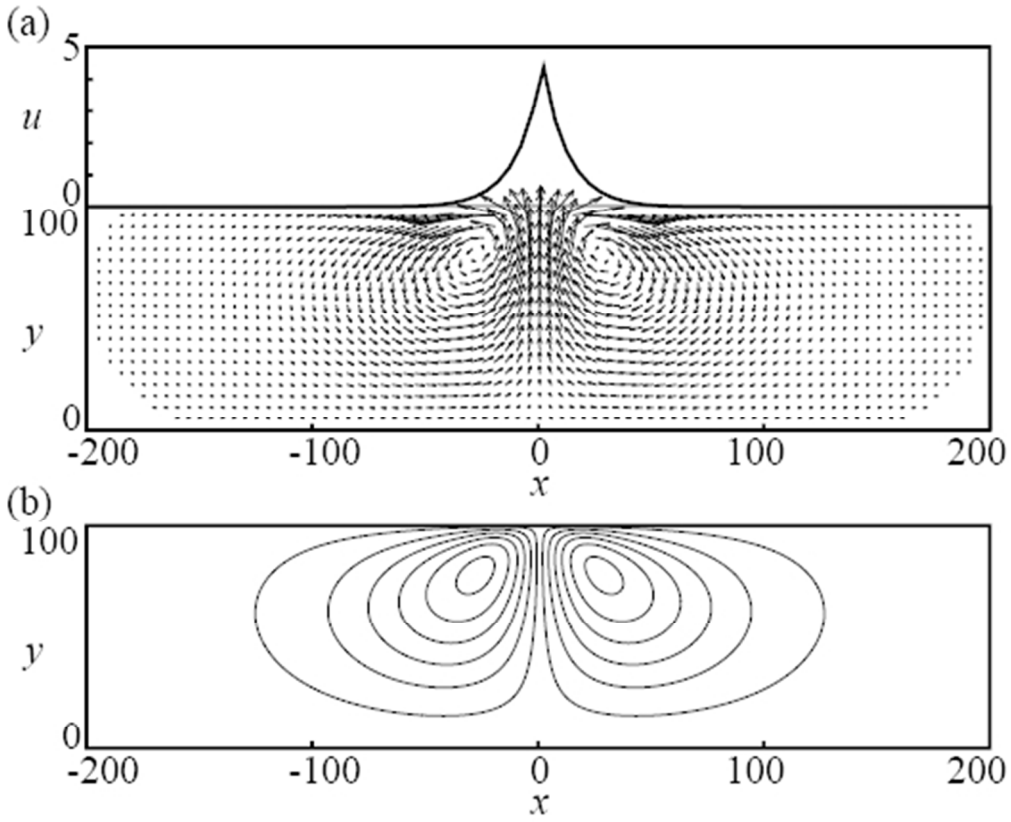

88x73mm (150 x 150 DPI)

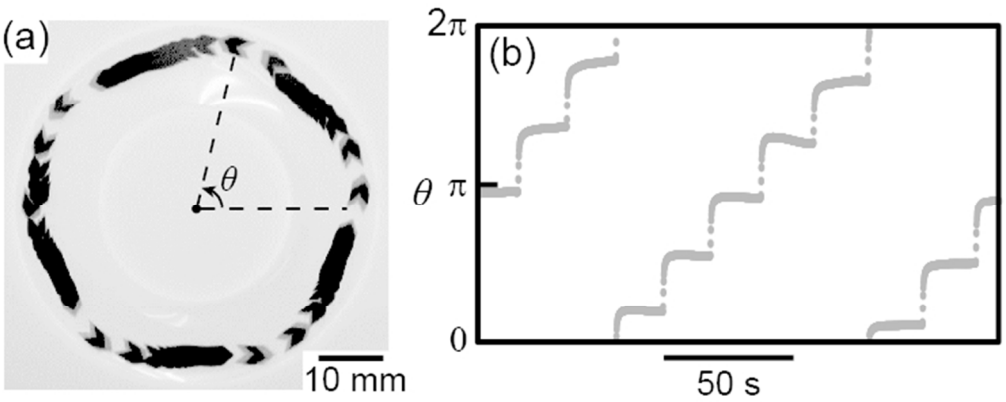

124x50mm (150 x 150 DPI)

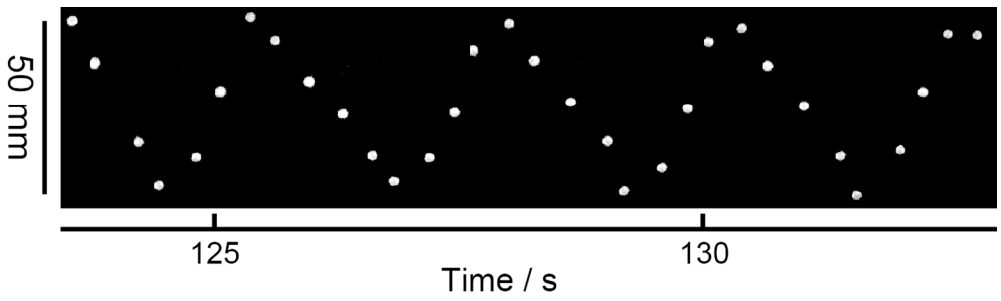

289x85mm (150 x 150 DPI)

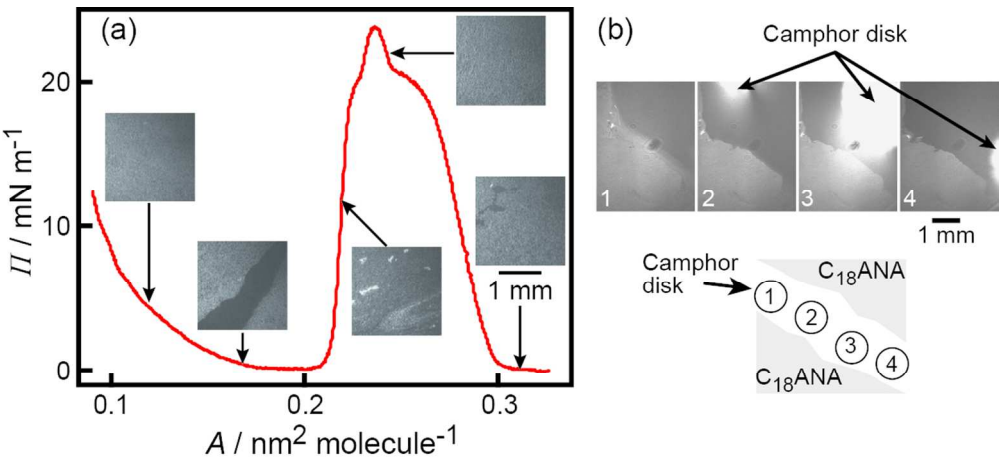

211x96mm (150 x 150 DPI)

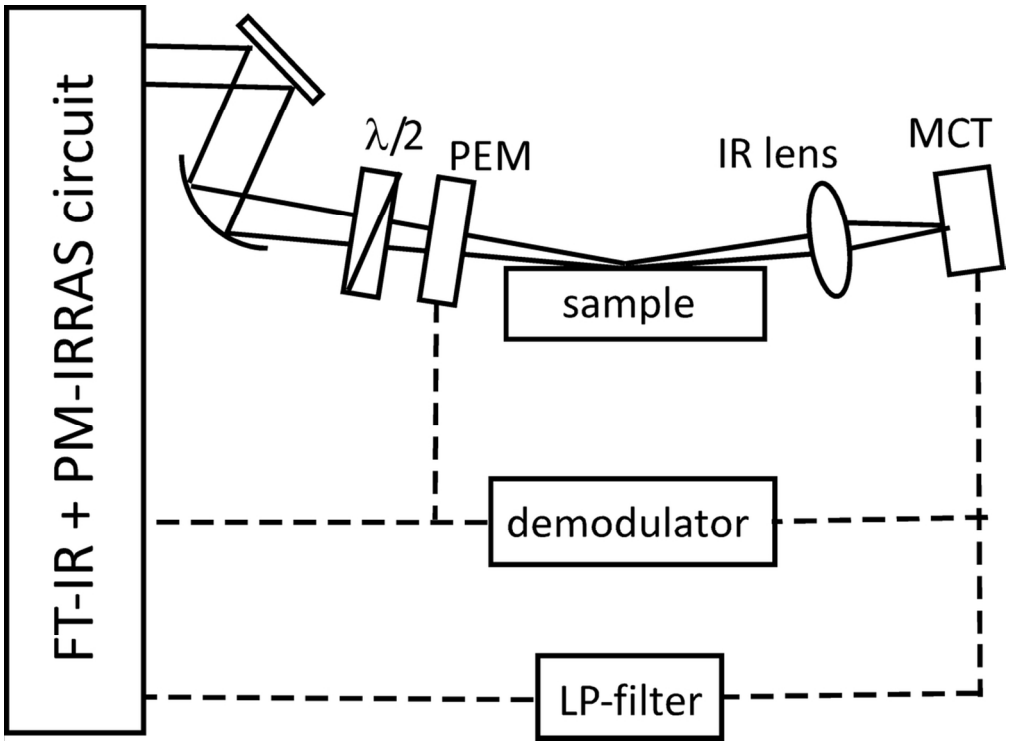

102x75mm (300 x 300 DPI)

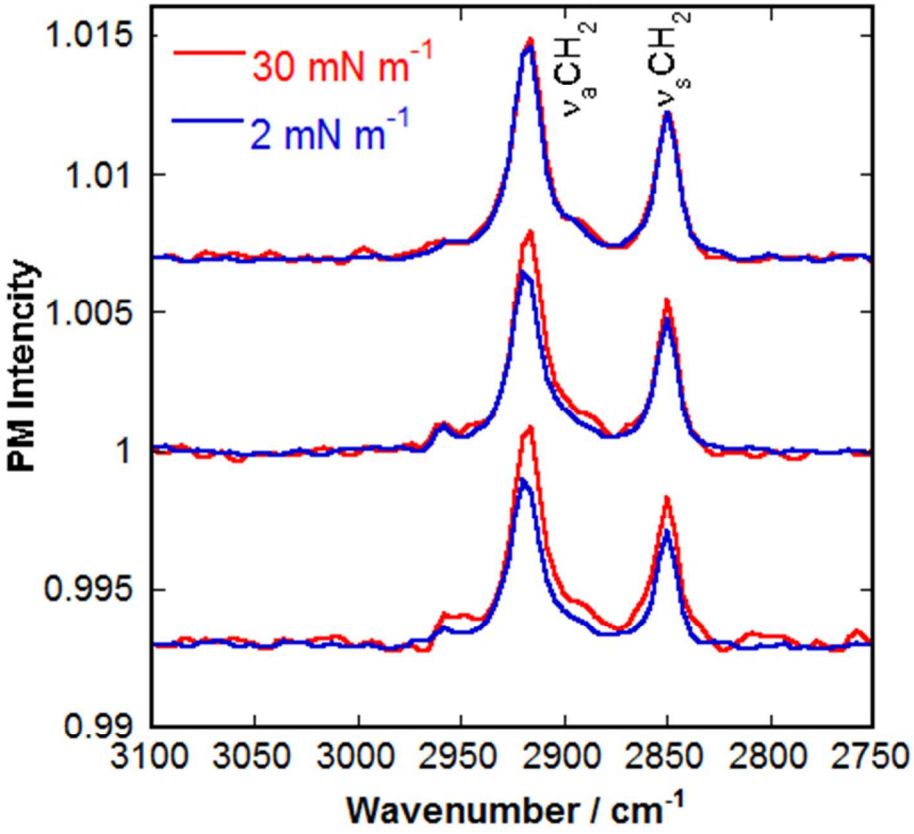

163x152mm (72 x 72 DPI)

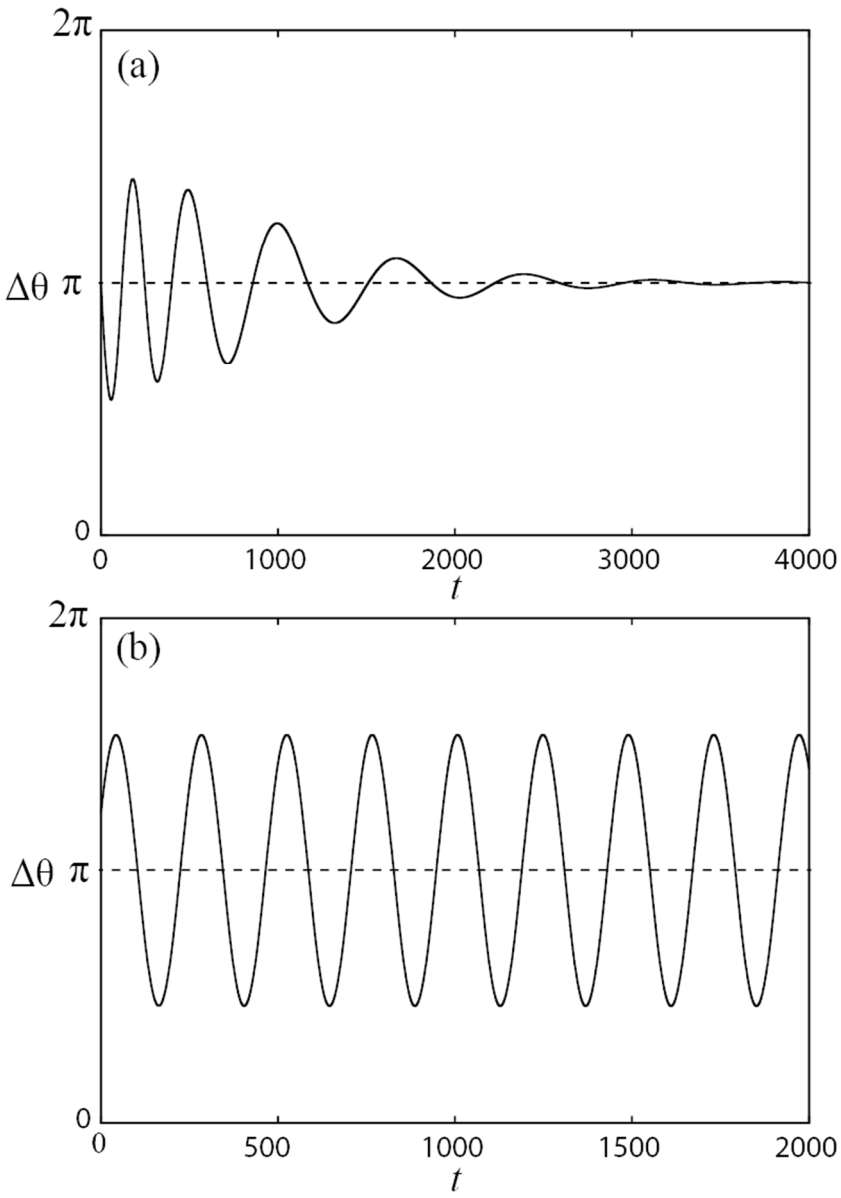

133x192mm (150 x 150 DPI)

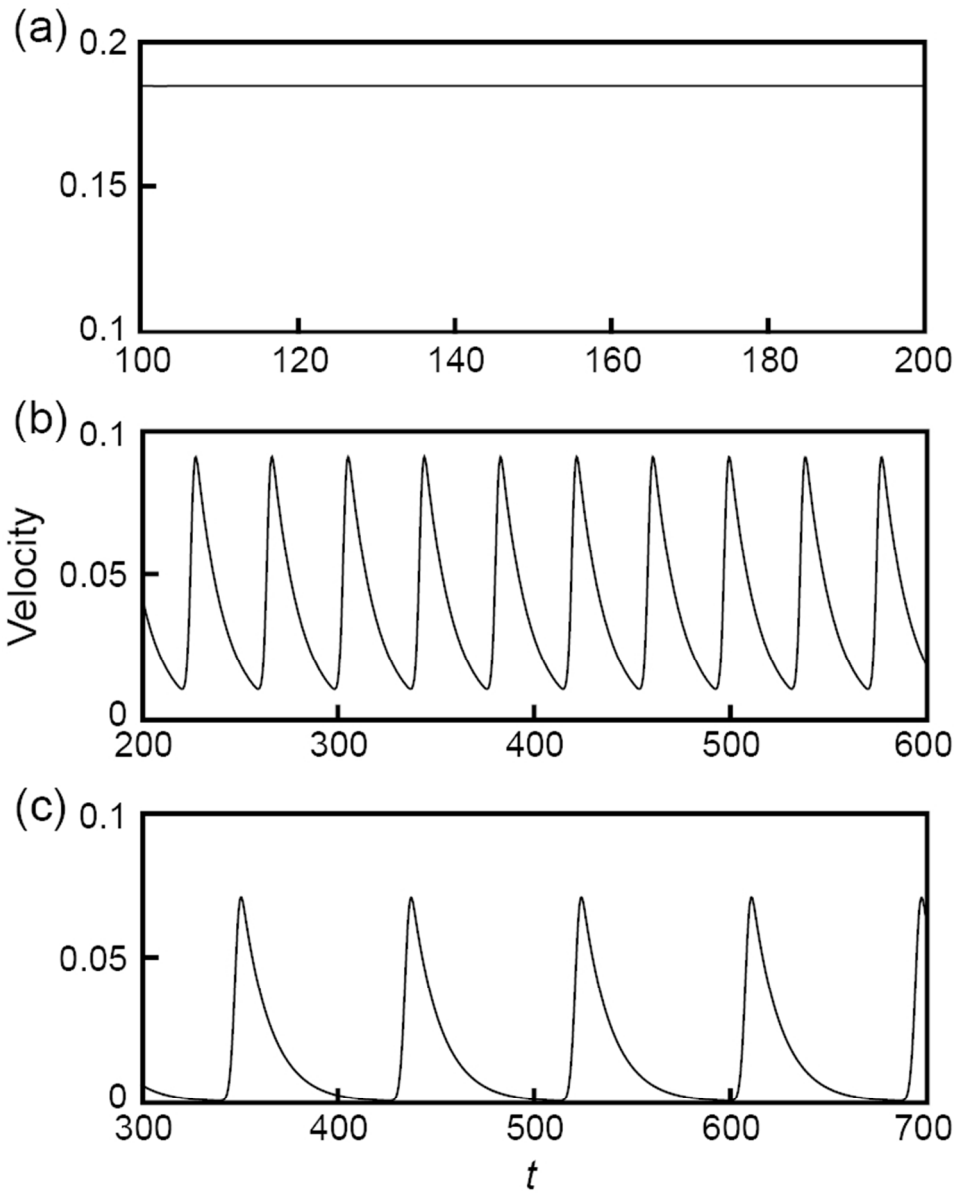

132x166mm (150 x 150 DPI)

Reaction	Self-propelled solid object	Reactant in the aqueous phase	Features of motion depending on [reactatnt]	Ref.
acid-base	camphoric acid	HPO_4^{2-} (base)	**C → O → N**	76, 77
redox	benzoquinone	ascorbic acid or NADPH	**C → O → N**	78, 81
complex formation	1,10-phenanthroline	Fe^{2+} (metal ion)	**C → O → C**	79, 80
enzyme	benzoquinone	G6PDH	**C → O → N**	81

137x53mm (150 x 150 DPI)